Stability of Hysteretic Controlled Voltage Source Converters in a Power System

Arindam Ghosh, *Fellow, IEEE* and Gerard Ledwich, *Senior Member, IEEE*

ABSTRACT: This paper develops a tool for the stability analysis of hysteretic controlled voltage source converters that are connected to a power system. Each VSC is controlled by a state feedback control input to a hysteretic comparator. A suitable model of the converter is first developed by including the state feedback gains and hysteretic switching controller design. The model is then extended to incorporate parallel operation of two VSCs. To consider autonomous operation, droop controllers are incorporated in the model. A linearized model of the system is developed for eigen analysis. It has been shown that the system response predicted by the developed model matches PSCAD simulation results very closely. Since hysteretic control is widely used for commercial converters, the model developed can be used as an analytical tool.

Index Terms: Voltage source converters, autonomous operation, linear quadratic control, stability analysis.

I. INTRODUCTION

IN THE PAST few decades, the use of power converters, has become more common in uninterrupted power supply (UPS) application as well as in interfacing the micro sources in a distributed generation (DG) system. In a UPS application, the parallel operation of the converters can provide solution to improve capability, reliability and redundancy. In a distributed generation system, the micro sources, especially the intermittent types (like wind and solar), are interfaced through voltage source converters (VSCs) to the network [1].The converter can be used to maximize the energy yield from the micro source, control of output power and to improve power quality. The parallel connected converters control the power flow and quality by controlling the power conversion between the dc bus and the available grid [2].

Current regulator instability in parallel VSCs has been discussed in [3], in which a simple method of paralleling structures with carrier-based PWM current regulators to independently regulate each inverter's current is employed. The instability between the parallel inverters and the common motor can result in large uncontrolled currents, when the current regulators enter PWM overmodulation region, resulting in a loss of current control.

A current/load sharing mechanism has to be employed to avoid the overloading of any converters, especially when multiple converters operate in an autonomous mode. Control of output power using output feedback is commonly used. Since the output currents of the converters are regulated at every switching instant, even with the harmonics in the output current, converters can share the current as desired.

The authors thank CRISRO Cluster on Intelligent Grid for the financial support to carry on the project.

A. Ghosh and G. Ledwich Zare are with the School of Engineering Systems, Queensland University of Technology, Brisbane, Qld 4001, Australia.

Email: a.ghosh@qut.edu.au

The load sharing or the real and reactive power sharing can be achieved by controlling two independent quantities – frequency and the fundamental voltage magnitude [4, 5]. In [4], a control method for a converter feeding real and reactive power into a stiff system with a defined voltage is proposed, while [5] proposes a control scheme to improve the system transient stability. Both the paper uses frequency droop characteristics. In this paper however an angle droop is used as the power sharing mechanism [6].

A multi-converter system with instantaneous power sharing control is effectively a high order multi variable system. The VSCs should be controlled in such a manner that ensures a stable operation of the system. The system stability during load sharing has been further explored in [7-10]. Transient stability of a power system with high penetration level of power electronics interfaced (converter connected) distributed generation is explored in [7]. In [8], small-signal stability analysis of the combined droop and average power method for load sharing control of multiple distributed generation systems (DGs) in a stand-alone ac supply mode is discussed. The overall dynamics of the regulated converter is described in [9], where the characterization of regulated converters is addressed to enable the assessment of the stability, performance, supply and load interactions as well as transient responses. The stability analysis in autonomous operation is shown in [10] in a hybrid system, where a wind-PV-battery system is feeding an isolated single-phase load.

In this paper, the theory for the analysis of hysteretic VSCs operating in a power system is developed. Under mild assumptions, the standard line dynamic analysis tools such as eigen-study become possible. There are two main tools available to analyze converters operating in power systems. The first uses controlled fundamental frequency voltage sources, which ignores transients associated with the connecting filters [11]. The second approach uses the switch state averaging of pulse width modulated signals [12]. The quality of the hysteretic converter modeling is demonstrated in this paper on the special case of two VSCs closely connected. The novel contribution of this paper is that the widely used hysteretic converters can now be modeled as a part of a power system using linear tools.

In this paper, we have developed and verified the hysteretic converter model step-by-step. The converter structure and its control are discussed for a single converter in Section II. The mathematical model of a single hysteretic VSC is developed in Section III. The model not only includes the hysteretic switching controller, but also develops the reference values and the transformation of the state space equation to a common reference frame. In Section IV, two such converter models are combined to verify the operation when two VSCs are operating in parallel. The model for the parallel operation of two

VSCs is further developed to include the power sharing based on droop equations in Section V. In Section VI, the model of the two VSCs, operating in parallel and sharing power through droop equations, is linearized. Based on the linearized model, the eigenvalues are derived and compared with results obtained from a detailed switching time domain simulation.

II. Converter Structure and Control

In the analysis presented below, the uppercase letters indicate rms values, while the lowercase letters indicate instantaneous values. In this paper, all the DGs are assumed to consist of ideal dc voltage source supplying a voltage of V_{dc} to a VSC. The structure of the VSC is shown in Fig. 1. The VSC contains three H-bridges that are supplied from the common dc bus. The outputs of the H-bridges are connected to three single-phase transformers that are connected in wye for required isolation and voltage boosting [13]. The resistance R_T represents the switching and transformer losses, while the inductance L_T represents the leakage reactance of the transformers. The filter capacitor C_f is connected to the output of the transformers to bypass switching harmonics, while L_f represents an added output inductance of the DG system. Together L_T, C_f and L_f form an LCL or T-filter.

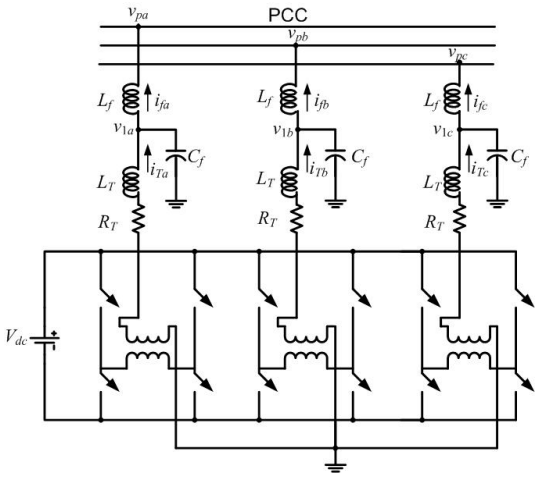

Fig. 1. Converter structure.

The equivalent circuit of one phase of the converter is shown in Fig. 2. In this, $u \cdot V_{dc}$ represents the converter output voltage, where u is the switching function and is given by $u = \pm 1$. The main aim of the converter control is to generate u. From the circuit of Fig. 2, the following state vector is chosen

$$z^T = \begin{bmatrix} i_T & i_f & v_c \end{bmatrix} \tag{1}$$

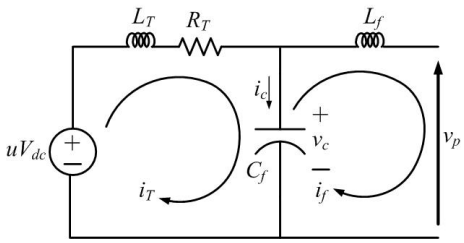

Fig. 2. Single-phase equivalent circuit of VSC.

Then the state space equation of the system can be written as

$$\dot{z} = Az + Bu + Cv_p \tag{2}$$

where u is the switching function and

$$A = \begin{bmatrix} -R_T/L_T & 0 & -1/L_T \\ 0 & 0 & 1/L_f \\ 1/C_f & -1/C_f & 0 \end{bmatrix}, B = \begin{bmatrix} V_{dc}/L_T \\ 0 \\ 0 \end{bmatrix}, C = \begin{bmatrix} 0 \\ -1/L_f \\ 0 \end{bmatrix}$$

The main aim of the converter control is to generate u_c from a suitable state feedback control law such that the output voltage and current are tracked properly according to their references. It is easy to generate references for the output voltage v_c and current i_f from the fundamental power flow requirements However, the same cannot be said about the reference for the current i_T [2]. On the other hand, once the reference for v_c is obtained, it is easy to calculate a reference for the current i_c through the filter capacitor (see Fig. 2).

To facilitate this, we define a new state vector as [2]

$$x^T = \begin{bmatrix} i_c & i_f & v_c \end{bmatrix} \tag{3}$$

We then have the following state transformation matrix

$$x = \begin{bmatrix} 1 & -1 & 0 \\ 0 & 1 & 0 \\ 0 & 0 & 1 \end{bmatrix} z = C_P z \tag{4}$$

The transformed state space equation is then given by combining (2) and (4) as

$$\dot{x} = C_p A C_p^{-1} x + C_p B u + C_p C v_p \tag{5}$$

If the system of (5) is sampled with a sampling time of ΔT, then its discrete-time description can be written in the form

$$x(k+1) = Fx(k) + Gu(k) + Hv_p(k) \tag{6}$$

To control the converter, we shall employ a discrete time linear quadratic regulator (LQR), which minimizes the objective function

$$J = \sum \left[x(k) - x_{ref}(k)\right]^T Q \left[x(k) - x_{ref}(k)\right] + r^2 u_c(k)$$

to obtain the control of the form

$$\begin{aligned} u_c(k) &= -K\left[x(k) - x_{ref}(k)\right] \\ &= \begin{bmatrix} k_1 & k_2 & k_3 \end{bmatrix} \left[x_{ref}(k) - x(k)\right] \\ &= k_1\left(i_{cref} - i_c\right) + k_2\left(i_{fref} - i_f\right) + k_3\left(v_{cref} - v_c\right) \end{aligned} \tag{7}$$

where x_{ref} is the reference vector and K is the feedback gain matrix. From $u_c(k)$, the switching function is generated as

$$\begin{aligned} &\text{If } u_c(k) > h \text{ then } u = +1 \\ &\text{elseif } u_c(k) < -h \text{ then } u = -1 \end{aligned} \tag{8}$$

where h is a small number.

A Linear Quadratic Regulator is shown to produce an infinite gain margin and a phase margin of at least 60° [14]. This has been used in [2] robust hysteretic LQR state feedback

switching controller. The following example demonstrates the effectiveness of this control.

Example 1: In this example, let us assume that the VSC of Fig. 1 is connected to an infinite bus at the PCC. The system parameters considered for the study are given in Table I. To design the discrete-time controller, we have chosen a diagonal state weighting matrix as Q = diag(1 1000 10) and the control weighting as r = 0.01. This choice of Q emphasizes a maximum tracking effort on i_f and a minimum effort on i_c. The sampling time is chosen as 10 μs. The resultant gain matrix is K = [0.4338 8.3977 0.8405].

The desired converter output voltage is 11 kV (L-L, rms) (which translates into an instantaneous phase voltage of 8.98 kV peak) with a phase angle of 30° with respect to PCC voltage. This sets the references of the currents from simple circuit laws. The peak of i_f reference is 59.195 A with an angle of 15°, while the peak of i_c reference is $\omega C_f 9.98\times10^3$ A and its phase angle 60°, i.e., leading v_c by 30°. The nine instantaneous reference quantities (3 for each phase are formed) and are tracked using the control law given in (7) and (8).

Table-I: System parameters for Example 1.

System Quantities	Values
Systems frequency	50 Hz
PCC voltage V_p	11 kV (L-L, rms)
PCC voltage phase	0° (Reference)
DC voltage V_{dc}	3.0 kV
Single-phase transformers	3//11 kV, with 10% leakage reactance (L_T = 31.8 mH)
Transformer losses R_T	0.1 Ω
Filter capacitor C_f	50 μF
Filter inductance L_f	250 mH

This simulation and all the subsequent PSCAD simulations use an integration step size of 10 μs. Each VSC is modeled by IGBTs and anti-parallel diodes, with their associated RC snubber circuits. Each IGBT or diode is modeled by its on and off resistance, forward voltage drop, forward breakover voltage, reverse withstanding voltage and snubber parameters. The average switching frequency is 15 kHZ.

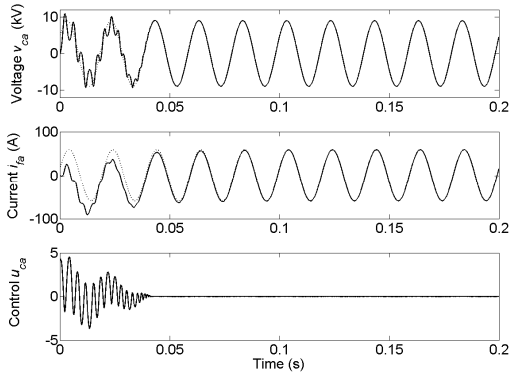

Fig. 3. Voltage and current tracking in Example 1.

The results are shown in Fig. 3, which shows the results of only one phase. The behavior of the other two phases is similar and is not shown here. Phase-a converter output voltage (v_{ca}) and the injected currents (i_{fa}) and their references (dotted lines) are shown in this figure, along with the control input u_{ca}. It can be seen that the control input reaches the zero value within 2½ cycles (0.05 s). From (7), u_c = 0 corresponds to a sliding plane in (i_c, i_f, v_c) space. With LQR design of the gain matrix, this usually implies the rapid convergence to the references as evident from Fig. 3.

During the initial reaching phases, the control input spends effort in trying to reach the sliding plane. Once the converter control reaches the sliding plane, its dynamics can be modeled as a reduced order linear system, which is described in the next section.

III. Mathematical Model of a VSC

In this section, a composite model of the converter in the d-q domain is developed, which also includes the controller. Traditional sliding mode design consider a function S and control such that $S\dot{S} \le 0$. Then the system will approach S = 0, which is called the sliding line [15, 16]. When a finite switch rate constraint is applied, the system will chatter around S = 0, at the switching frequency. Provided that the switch frequency is sufficiently high, the power system impact at switch frequency will be negligible. We also assume that the load disturbances are small enough that the rate of change of current is within the capability of the converter thus the model of the system being on the sliding line will be valid.

A. Converter Model

From equivalent circuit shown in Fig. 2, the following equations are obtained for each of the phases of the three-phase system

$$\frac{di_T}{dt} = -\frac{R_T}{L_T} i_T + \frac{\left(-v_c + u_c.V_{dc}\right)}{L_T} \tag{9}$$

$$\frac{dv_c}{dt} = \frac{\left(i_T - i_f\right)}{C_f} \tag{10}$$

$$v_c - v_p = L_f \frac{di_f}{dt} \tag{11}$$

Equations (9-11) are transformed into a *d-q* reference frame of converter output voltages, rotating at system frequency ω, where *a-b-c* to *d-q* transformation matrix P is given by

$$P = \frac{2}{3}\begin{bmatrix} \cos(\omega t) & \cos\left(\omega t - \frac{2\pi}{3}\right) & \cos\left(\omega t + \frac{2\pi}{3}\right) \\ -\sin(\omega t) & -\sin\left(\omega t - \frac{2\pi}{3}\right) & -\sin\left(\omega t + \frac{2\pi}{3}\right) \\ \frac{1}{2} & \frac{1}{2} & \frac{1}{2} \end{bmatrix} \tag{12}$$

Defining a state vector as

$$z_i = [i_{Td} \quad i_{Tq} \quad i_{fd} \quad i_{fq} \quad v_{cd} \quad v_{cq}]^T \tag{13}$$

the state equation in the *d-q* frame is given by

$$\dot{z}_i = A_{zi} z_i + B_{zi} u_{cdq} + C_{zi} v_{pdq} \tag{14}$$

where u_{cdq} and v_{tdq} are two vectors containing the d and q axis components of u_c and v_t and the matrices A_{zi},B_{zi} and C_{zi} are

obtained by combining (9)-(12). Let us now define a new state vector as

$$x_i = [i_{cd} \quad i_{cq} \quad i_{fd} \quad i_{fq} \quad v_{cd} \quad v_{cq}]^T \tag{15}$$

Then using a transformation similar to (4), we get the following state equation

$$\dot{x}_i = A_i x_i + B_i u_{dq} + C_i v_{pdq} \tag{16}$$

From (7), the d and q components of the sliding plane are given as

$$\begin{bmatrix} u_{cd} \\ u_{cq} \end{bmatrix} = H_i \left(x_{refdq} - x_i \right) = \begin{bmatrix} S_d \\ S_q \end{bmatrix} \tag{17}$$

where

$$H_i = \begin{bmatrix} k_1 & 0 & k_2 & 0 & k_3 & 0 \\ 0 & k_1 & 0 & k_2 & 0 & k_3 \end{bmatrix}$$

$$x_{refdq} = [i_{cdref} \quad i_{cqref} \quad i_{fdref} \quad i_{fqref} \quad v_{cdref} \quad v_{cqref}]^T$$

To analyze the system, we transform the state variables to a new vector w as

$$w_i = [S_d \quad S_q \quad i_{fd} \quad i_{fq} \quad v_{cd} \quad v_{cq}]^T \tag{18}$$

Then, from (17), the states of (15) can be written in terms of (18) as

$$w_i = \begin{bmatrix} -H_i \\ 0_{4\times 2} \quad I_4 \end{bmatrix} x_i + \begin{bmatrix} H_i \\ 0_{4\times 6} \end{bmatrix} x_{refdq} = T_i x_i + F_i x_{refdq} \tag{19}$$

where $0_{n\times m}$ is an $n\times m$ null matrix and I_n is $n\times n$ identity matrix. From the above we get the two following equations

$$x_i = T_i^{-1} \left(w_i - F_i x_{refdq} \right) \tag{20}$$

$$\dot{w}_i = T_i \dot{x}_i + F_i \dot{x}_{refdq} \tag{21}$$

From (16) and (21), we get

$$\dot{w}_i = T_i \left(A_i x_i + B_i u_{dq} + C_i v_{pdq} \right) + F_i \dot{x}_{refdq} \tag{22}$$

Substituting (20) in (22), we get

$$\begin{aligned} \dot{w}_i = {} & T_i A_i T_i^{-1} w_i - T_i A_i T_i^{-1} F_i x_{refdq} + T_i B_i u_{dq} \\ & + T_i C_i v_{pdq} + F_i \dot{x}_{refdq} \end{aligned} \tag{23}$$

Since u_{dq} is chosen such that $S_d = S_q = 0$, we can eliminate them from the state vector w_i

Let us define a new state operator such that

$$y_i = \begin{bmatrix} i_{fd} & i_{fq} & v_{cd} & v_{cq} \end{bmatrix}^T = N_i w_i \tag{24}$$

where $N_i = \begin{bmatrix} 0_{4\times 2} & I_4 \end{bmatrix}$. Now since $w_i = N_i^T y_i$ and $N_i F_i = N_i T_i B_i = 0$, (23) can be re-expressed as

$$\dot{y}_i = \overline{A}_i y_i + \overline{B}_i x_{refdq} + \overline{C}_i v_{pdq} \tag{25}$$

where

$$\overline{A}_i = N_i T_i A_i T_i^{-1} N_i^T, \; \overline{B}_i = -N_i T_i A_i T_i^{-1} F_i, \; \overline{C}_i = N_i T_i C_i$$

B. Computation of References

To solve the state equation (25), the reference vector x_{refdq} is required as input. In this sub-section, we shall discuss how they can easily be written in terms of the known quantities. We must however remember that all the d-q quantities are expressed in the reference frame of the converter output voltages. Let us define the three-phase instantaneous reference converter output voltages as

$$\begin{aligned} & v_{caref} = V_{cm} \sin(\omega t), \quad v_{cbref} = V_{cm} \sin(\omega t - 120^\circ), \\ & v_{ccref} = V_{cm} \sin(\omega t + 120^\circ) \end{aligned}$$

Then the transformation (12) will result in

$$\begin{bmatrix} v_{cdref} \\ v_{cqref} \end{bmatrix} = \begin{bmatrix} 0 \\ -V_{cm} \end{bmatrix} \tag{26}$$

Consequently, the reference for the capacitor currents that are leading the corresponding voltages by 90° are given as

$$\begin{bmatrix} i_{cdref} \\ i_{cqref} \end{bmatrix} = \begin{bmatrix} V_{cm} \omega C_f \\ 0 \end{bmatrix} \tag{27}$$

The expression for the power and reactive power are given by

$$P = \frac{3}{2} \left(v_d i_d + v_q i_q \right) \tag{28}$$

$$Q = \frac{3}{2} \left(v_q i_d - v_d i_q \right) \tag{29}$$

Let the real and reactive power that are desired to be injected to the PCC by the converter be denoted respectively by P_{ref} and Q_{ref}. Then from (26), (28) and (29), we can write

$$\begin{bmatrix} i_{fdref} \\ i_{fqref} \end{bmatrix} = -\frac{2}{3V_{cm}} \begin{bmatrix} Q_{ref} \\ P_{ref} \end{bmatrix} \tag{30}$$

Combining (26), (27) and (30) we form the reference vectors in terms of V_{cm}, P_{ref} and Q_{ref}.

C. Transformation into a Common Reference Frame

The reference quantities are defined in terms of the reference frame of the converter output voltage. These need to be converted into a common reference frame. Let us choose the PCC voltage as the common reference frame D-Q. Let also the angle between the PCC voltage and the converter voltage be δ. Then the relation between these two frames is shown in Fig. 4. From these figure we can write

$$\begin{bmatrix} f_D \\ f_Q \end{bmatrix} = \begin{bmatrix} \cos\delta & -\sin\delta \\ \sin\delta & \cos\delta \end{bmatrix} \begin{bmatrix} f_d \\ f_q \end{bmatrix} = T \begin{bmatrix} f_d \\ f_q \end{bmatrix} \tag{31}$$

All the reference d-q quantities are pre-multiplied by T to transform them in D-Q frame. The converter equation (25) can then be re-written as

$$\dot{y}_i = \overline{A}_i y_i + \overline{B}_i x_{refDQ} + \overline{C}_i v_{pDQ} \tag{32}$$

Note that the states also get transformed into D-Q. However the subscripts are avoided here for brevity.

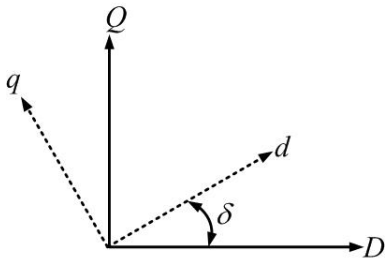

Fig. 4. Relation between d-q and D-Q frames.

Example 2: The system parameters chosen for this example are the same as those given in Example 1. For this case, the real and reactive power injected by the converter are 770.3 kW and 206.4 kVAr respectively. The time response of the state equations (32) is obtained using MATLAB. The converter output voltages and injected currents are shown in Fig. 5. It can be seen that the steady state response of these quantities are almost identical to those of Fig. 3.

Comparing the responses in Figs. 3 and 5, it can be seen that they differ in the initial starting period. During this period, the system is trying to reach the sliding plane. Once the system is on this plane, the two responses are nearly identical. This is illustrated in this above example. Once the system is on the sliding plane, it is robust to perturbations to system operating conditions, as will be illustrated in some of the subsequent examples. Therefore the model presented can be used for eigenvalue analysis and system response prediction.

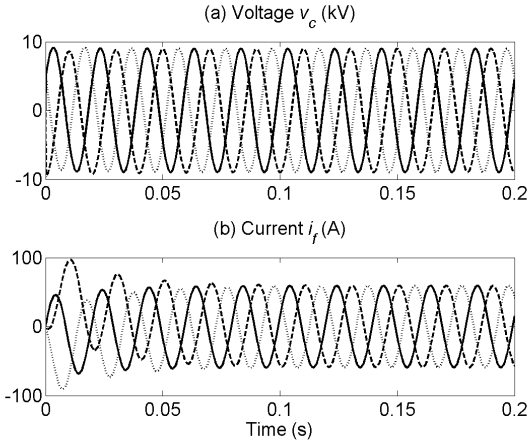

Fig. 5. Output voltage and injected current for Example 2.

IV. Mathematical Model of VSC Parallel Operation

The single-line diagram when two VSC operate in parallel is shown in Fig. 6. In this, the PCC is connected to an infinite bus with a voltage of v_s. A load, with an impedance of $R_L + j\omega L_L$ is connected to the PCC. The load current is denoted by i_L. The system parameters and quantities of the two VSCs are denoted by subscripts 1 and 2.

The state equations of the VSCs can be written in the form (32) as

$$\dot{y}_{i1} = \overline{A}_{i1} y_{i1} + \overline{B}_{i1} x_{ref\,1DQ} + \overline{C}_{i1} v_{pDQ} \tag{33}$$

$$\dot{y}_{i2} = \overline{A}_{i2} y_{i2} + \overline{B}_{i2} x_{ref\,2DQ} + \overline{C}_{i2} v_{pDQ} \tag{34}$$

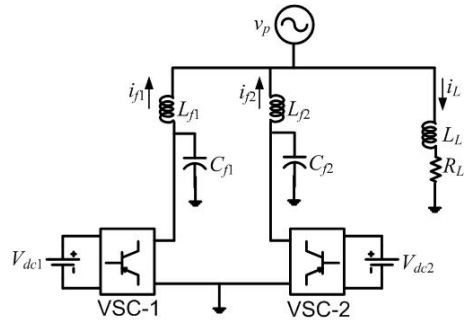

Fig. 6. Single-line diagram of parallel operation of two VSCs.

The state equations of the VSCs can be written in the form (32) as

$$\dot{y}_{i1} = \overline{A}_{i1} y_{i1} + \overline{B}_{i1} x_{ref\,1DQ} + \overline{C}_{i1} v_{pDQ} \tag{33}$$

$$\dot{y}_{i2} = \overline{A}_{i2} y_{i2} + \overline{B}_{i2} x_{ref\,2DQ} + \overline{C}_{i2} v_{pDQ} \tag{34}$$

Furthermore, the load current in D-Q component is given as

$$\frac{d}{dt}\begin{bmatrix} i_{LD} \\ i_{LQ} \end{bmatrix} = \begin{bmatrix} -R_L/L_L & \omega \\ -\omega & -R_L/L_L \end{bmatrix}\begin{bmatrix} i_{LD} \\ i_{LQ} \end{bmatrix} + \begin{bmatrix} 1/L_L & 0 \\ 0 & 1/L_L \end{bmatrix}\begin{bmatrix} v_{pD} \\ v_{PQ} \end{bmatrix} \tag{35}$$

Therefore defining a composite state vector as

$$x_t^T = \begin{bmatrix} y_{i1}^T & y_{i2}^T & i_{LD} & i_{LQ} \end{bmatrix}$$

we can combine (33)-(35) to form the overall state space equation of the system.

Example 3: Let us consider the system shown in Fig. 6. Both the VSCs have the same parameters and the PCC voltage the same as discussed in Examples 1 and 2. The load resistance is 48.2 Ω and the inductance is 0.3 H. At the beginning, the following are assumed

$$V_{c1ref} = \left|\frac{11}{\sqrt{3}}\right| \angle 30^\circ \text{ kV and } V_{c2ref} = \left|\frac{11}{\sqrt{3}}\right| \angle 20^\circ \text{ kV}$$

This implies that P_{1ref} and Q_{1ref} are the same as those given in Example 2, while P_{2ref} = 526.9 kW and Q_{2ref} = 92.9 kVAr. With the system operating in steady state with these values, the reference for VSC-2 is suddenly changed at 0.05 s. The peak of the voltage is reduced to 95% of the nominal value, while its phase angle is changed to 30°. The reference powers are P_{2ref} = 731.79 kW and Q_{2ref} = 122.9 kVAr. The system responses for VSC-2 are shown in Figs. 7 and 8, where the solid lines depict the MATLAB time domain results with the deduced model and the dotted lines depict the PSCAD outputs. In Fig. 7, the converter output voltages (v_{c2}) are shown. It can be seen that the PSCAD results are almost identical to those of MATLAB. For the injected currents (i_{f2}), the difference between the PSCAD simulation results and the predicted behaviors using MATLAB of are also very small.

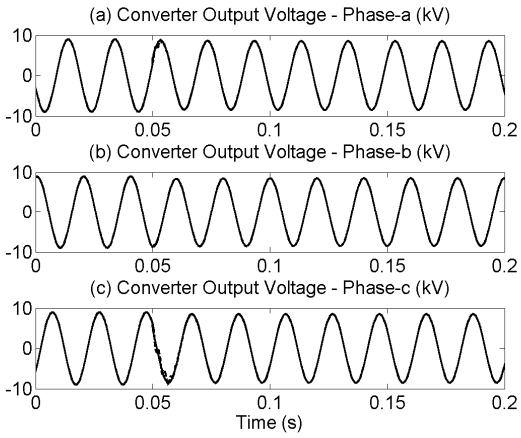

Fig. 7. Simulated and predicted output voltages of VSC-2.

V. Mathematical Model for Autonomous Operation

Let us now assume that the PCC is a floating source, i.e., the voltage source v_p in Fig. 6 is absent and the two converters operate in parallel to share the load through droop characteristics. We shall use an angle droop based on the active power and a voltage magnitude droop based on reactive power [6].

$$\begin{aligned}\delta &= \delta_{rated} - m\times(P_e - P_{rated})\\ V_{cm} &= V_{cm-rated} - n\times(Q_e - Q_{rated})\end{aligned} \tag{36}$$

where $V_{cm\text{-}rated}$ and δ_{rated} are the rated voltage magnitude and angle respectively of a VSC when it is supplying the load to its rated power levels of P_{rated} and Q_{rated}.

Calculating real and reactive power from instantaneous measurements can often lead to ripple in these quantities that will cause ripple in the converter references. To avoid this, the real and reactive power are passed through low pass filters before they are used in the droop equations. These low pass filters are described in frequency domain as

$$P_e = \frac{\omega_c}{s+\omega_c}P \quad Q_e = \frac{\omega_c}{s+\omega_c}Q \tag{37}$$

where P and Q are instantaneous measured values and P_e and Q_e are their respective filtered outputs. We now substitute these values and δ and V_{cm} in (26), (27) and (30).

Since the PCC is not connected to an infinite bus, we have to eliminate the vector v_{pDQ} from the state equation. From (35), we can write

$$\begin{bmatrix} v_{pD}\\ v_{PQ}\end{bmatrix} = L_L\frac{d}{dt}\begin{bmatrix} i_{LD}\\ i_{LQ}\end{bmatrix} - L_L\begin{bmatrix} -R_L/L_L & \omega\\ -\omega & -R_L/L_L\end{bmatrix}\begin{bmatrix} i_{LD}\\ i_{LQ}\end{bmatrix} \tag{38}$$

Again, using Kirchoff's current law (KCL) at PCC, we get

$$i_{LD} = i_{f1D} + i_{f2D} \text{ and } i_{LQ} = i_{f1Q} + i_{f2Q} \tag{39}$$

Let us now define a new set of state vectors that contain only the state equations of the two converters. This is given by

$$x_c^T = \begin{bmatrix} y_{i1}^T & y_{i2}^T\end{bmatrix}$$

We can then express (38) in terms of the above state vector and its derivative as

$$\begin{bmatrix} v_{pD}\\ v_{PQ}\end{bmatrix} = A_P\dot{x}_c + B_P x_c \tag{40}$$

where the matrices A_p and B_p both have dimensions (2×8) and are computed from (38) and (39). From (33), (34) and (40), the model for the autonomous operation of the two VSCs is derived as

$$\begin{aligned}\dot{x}_c = &\begin{bmatrix}\overline{A}_{i1} & 0_{4\times4}\\ 0_{4\times4} & \overline{A}_{i2}\end{bmatrix}x_c\\ &+\begin{bmatrix}\overline{B}_{i1} & 0_{4\times6}\\ 0_{4\times6} & \overline{B}_{i2}\end{bmatrix}x_{crefDQ} + \begin{bmatrix}\overline{C}_{i1}\\ \overline{C}_{i2}\end{bmatrix}\left(A_P\dot{x}_c + B_P x_c\right)\end{aligned} \tag{41}$$

The above equation can be regrouped to form the state space equations for the autonomous operation of the VSCs as

$$\dot{x}_c = A_c x_c + B_c x_{crefDQ} \tag{42}$$

where

$$E = I_8 - \begin{bmatrix}\overline{C}_{i1}\\ \overline{C}_{i2}\end{bmatrix}A_P,\ A_c = E^{-1}\left(\begin{bmatrix}\overline{A}_{i1} & 0_{4\times4}\\ 0_{4\times4} & \overline{A}_{i2}\end{bmatrix} + \begin{bmatrix}\overline{C}_{i1}\\ \overline{C}_{i2}\end{bmatrix}B_P\right)$$

$$B_c = E^{-1}\begin{bmatrix}\overline{B}_{i1} & 0_{4\times6}\\ 0_{4\times6} & \overline{B}_{i2}\end{bmatrix}$$

Example 4: Let us consider the same system discussed in Example 3, except the voltage source v_{ps}, is removed. Also the filter inductance of VSC-2 is chosen as 0.3125 H for desired power sharing. The droop coefficients from (36) are chosen as

$$m_1 = 0.1\,\text{rad/MW and } m_2 = 0.125\,\text{rad/MW}$$
$$n_1 = 0.01\,\text{kV/MVAr and } n_2 = 0.0125\,\text{kV/MVAr}$$

The cutoff frequency for the low pass filters are chosen as ω_c = 31.4 rad/s. With the system operating in steady state with a load resistance is of 48.2 Ω and the inductance of 0.3 H, the load impedance is halved at 0.1 s. The results are shown in Figs. 8 to 10. In all these figures, the MATLAB time domain results based on the model (42) and PSCAD simulation results are shown in sub-figures (a) and (b) and the errors between them are shown in (c). In Fig. 8, the output voltage for phase-a of VSC-2 is shown. It can be seen that the maximum error between the MATLAB prediction and PSCAD simulation are less than 30 V, while the peak of the phase voltage is nearly 9 kV. This implies that the error is less than 0.33%. The error in the converter output (injected) current is less than 0.2 A (0.4%). The output powers of the two converters are shown in Fig. 9. The errors are less than 0.5%. From the reactive power plot shown in Fig. 10, it can be seen that the errors are less than 0.1 %. Therefore the prediction is fairly accurate.

VI. Small Signal Model for Eigen Analysis

Since the system response obtained by the mathematical model closely matches that of the PSCAD simulation, the VSC model developed in the previous sections can be used to find an autonomous small signal model of the system discussed in the previous section. To facilitate this, we must eliminate the reference vector from (42).

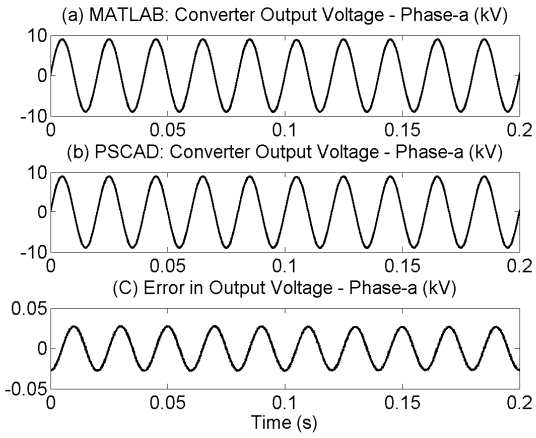

Fig. 8. VSC-2 output voltage of phase-a and its error.

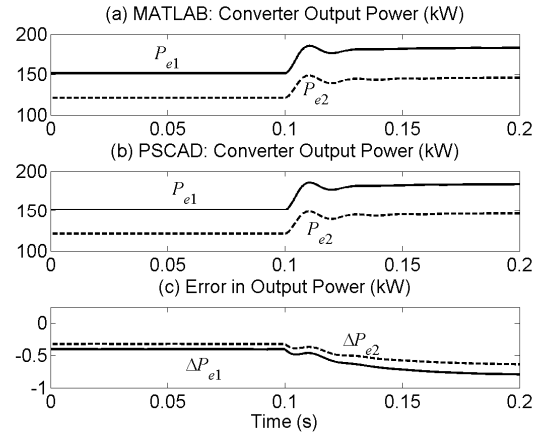

Fig. 9. Output active power of the converters and their error.

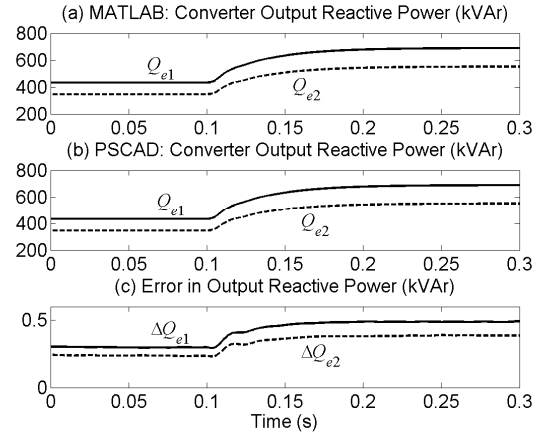

Fig. 10. Output reactive power of the converters and their error.

From (37), (28) and (29), we can write

$$\begin{aligned}\dot{P}_e &= -\omega_c P_e + \frac{3\omega_c}{2}\left(v_{cd} i_{fd} + v_{cq} i_{fq}\right)\\ \dot{Q}_e &= -\omega_c Q_e + \frac{3\omega_c}{2}\left(v_{cq} i_{fd} - v_{cd} i_{fq}\right)\end{aligned} \tag{43}$$

Linearization of the above equations yield

$$\begin{aligned}\Delta\dot{P}_e &= -\omega_c \Delta P_e + \frac{3\omega_c}{2}\left(v_{cd0}\Delta i_{fd} + i_{fd0}\Delta v_{cd} + v_{cq0}\Delta i_{fq} + i_{fq0}\Delta v_{cq}\right)\\ \Delta\dot{Q}_e &= -\omega_c \Delta Q_e + \frac{3\omega_c}{2}\left(v_{cq0}\Delta i_{fd} + i_{fd0}\Delta v_{cq} - v_{cd0}\Delta i_{fq} - i_{fq0}\Delta v_{dq}\right)\end{aligned} \tag{44}$$

where the suffix Δ defines a perturbed quantity and subscript 0 signifies the nominal values. Defining a vector of active and reactive powers as

$$x_{pq} = \begin{bmatrix} P_{e1} & Q_{e1} & P_{e2} & Q_{e2}\end{bmatrix}^T$$

equation (44) can be written as

$$\Delta\dot{x}_{pq} = A_{pq}\Delta x_{pq} + B_{pq}\Delta x_c \tag{45}$$

where A_{pq} = diag($-\omega_c$ $-\omega_c$ $-\omega_c$ $-\omega_c$) and B_{pq} can be derived from (44). We now replace the reference quantities by ΔP_e and ΔQ_e. To do that, we first linearize the droop equations (36) to obtain

$$\begin{aligned}\Delta\delta &= -m \times \Delta P_e\\ \Delta V_{cm} &= -n \times \Delta Q_e\end{aligned} \tag{46}$$

Then from (26) and (31) we get

$$\begin{bmatrix} v_{cDref}\\ v_{cQref}\end{bmatrix} = \begin{bmatrix}\cos\delta & -\sin\delta\\ \sin\delta & \cos\delta\end{bmatrix}\begin{bmatrix} 0\\ -V_{cm}\end{bmatrix}$$

Linearizing the above equation and substituting (46), we get

$$\begin{bmatrix}\Delta v_{cDref}\\ \Delta v_{cQref}\end{bmatrix} = \begin{bmatrix} -mV_{cmo}\cos\delta_0 & -n\sin\delta_0\\ -mV_{cm0}\sin\delta_0 & n\cos\delta_0\end{bmatrix}\begin{bmatrix}\Delta P_e\\ \Delta Q_e\end{bmatrix} \tag{47}$$

In a similar way, we find the references for the capacitor current are given as

$$\begin{bmatrix}\Delta i_{cDref}\\ \Delta i_{cQref}\end{bmatrix} = \begin{bmatrix}\lambda_1\sin\delta_0 & -\lambda_2\cos\delta_0\\ -\lambda_1\cos\delta_0 & -\lambda_2\sin\delta_0\end{bmatrix}\begin{bmatrix}\Delta P_e\\ \Delta Q_e\end{bmatrix} \tag{48}$$

where $\lambda_1 = m\omega C_f V_{cm0}$ and $\lambda_2 = n\omega C_f$. Finally replacing P_{ref} and Q_{ref} by P_e and Q_e respectively in (30), we get the linearized expressions for the injected currents as

$$\begin{bmatrix}\Delta i_{fDref}\\ \Delta i_{fQref}\end{bmatrix} = \frac{1}{V_{cm0}}\begin{bmatrix}\beta_{11} & \beta_{12}\\ \beta_{21} & \beta_{22}\end{bmatrix}\begin{bmatrix}\Delta P_e\\ \Delta Q_e\end{bmatrix} \tag{49}$$

where

$$\begin{aligned}\beta_{11} &= -(2/3)\left(mQ_{e0}\sin\delta_0 + mP_{e0}\cos\delta_0 - \sin\delta_0\right)\\ \beta_{12} &= -(2/3)\cos\delta_0 + ni_{fD0}\\ \beta_{21} &= -(2/3)\left(mP_{e0}\sin\delta_0 + \cos\delta_0 - mQ_{e0}\cos\delta_0\right)\\ \beta_{22} &= -(2/3)\sin\delta_0 + ni_{fQ0}\end{aligned}$$

We can then write the reference vector in (42) as

$$\Delta x_{crefDQ} = M_c \Delta x_{pq} \tag{50}$$

where the elements of M_c are obtained from (47)-(49). Combing (42), (45) and (50), we get a homogeneous state space description of the complete system as

$$\begin{bmatrix} \Delta\dot{x}_c \\ \Delta\dot{x}_{pq} \end{bmatrix} = \begin{bmatrix} A_c & B_c M_c \\ B_{pq} & A_{pq} \end{bmatrix} \begin{bmatrix} \Delta x_c \\ \Delta x_{pq} \end{bmatrix} \tag{51}$$

This homogenous model will be used for eigenvalue analysis.

Example 5: Let us consider the system discussed in Example 4. For eigenvalue analysis we vary a parameter m from 0.01×10^{-6} rad/W to 1.8×10^{-6} rad/W. Furthermore we choose the angle droop gains as $m_1 = m$ and $m_2 = 1.25\times m$. The plots of the dominant eigenvalues are shown in Fig. 13. The dominant eigenvalues cross imaginary axis at $m = 1.49022\times10^{-6}$ rad/W, which is pointed out in this figure. Also the oscillation frequency of the dominant eigenvalues is roughly 314 rad/s (50 Hz). From eigenvectors it has been determined that these eigenvalues are associated with real and reactive power supplied by the VSCs.

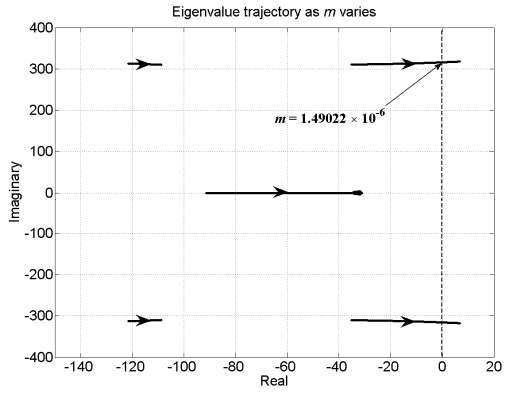

Fig. 13. Eigenvalues plots from stability analysis.

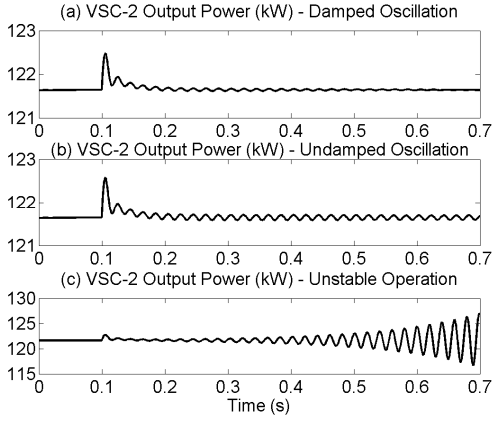

Fig. 14. VSC-2 output power showing stable, undamped and unstable

To validate the eigenvalue results, PSCAD simulations studies are carried out for the same system. With the system operating at steady state with the nominal values of droop gains given in example, the value of m is changed suddenly at 0.1 s. Fig. 14 shows the plots of the real power output of VSC-2 for three different values of m. Fig. 14 (a) shows a damped oscillation for $m = 1.3\times10^{-6}$ rad/W, for which all the eigenvalues are in the left half s-plane. Fig. 14 (b) shows sustained oscillation for $m = 1.49022\times10^{-6}$ rad/W, for which the dominant eigenvalues are on the imaginary axis. The unstable case for which the dominant eigenvalues are on the right half s-plane are shown in Fig. 14 (c) for $m = 1.8\times10^{-6}$ rad/W. Also notice that there are five peaks and five troughs in each 0.1 s, indicating that the oscillation frequency is 50 Hz. This fundamental frequency oscillation is also predicted by the eigenvalues.

VII. Conclusions

This paper develops a method for linear analysis of hysteretic controlled state feedback converters operating in power systems. One of the features of the proposed analysis is that state order is lower than those required for PWM converters. The process of analysis is illustrated using two VSCs that are connected at a bus. There is risk of oscillations of filter states the converters when they are connected at close proximity (e.g. in a microgrid). The robustness of the LQR based hysteretic design is able to be clearly shown using the eigenanalysis tool developed in this paper. The analysis process can be easily extended to include multiple converters, both hysteric and PWM controlled, that are connected to multiple buses of a power system.

References

[1] M. Reza, D. Sudarmadi, F. A. Viawan, W. L. Kling and L. Van Der Sluis, "Dynamic Stability of Power Systems with Power Electronic Interfaced DG," Power Systems Conference and Exposition, PSCE'06, pp. 1423-1428, 2006.

[2] A. Ghosh and G. Ledwich, "Load compensating DSTATCOM is weak ac systems," *IEEE Trans. Power Delivery*, Vol. 18, No. 4, pp. 1302-1309, 2003.

[3] J. Thunes, R. Kerkman, D. Schlegel and T. Rowan, "Current regulator instabilities on parallel voltage-source inverters," IEEE Trans. Industry Applications, Vol. 35, No. 1, pp. 70-77, 1999.

[4] M. C. Chandorkar, D. M. Divan and R. Adapa, "Control of parallel connected inverters in standalone ac supply systems," IEEE Trans. Industry Applications, Vol. 29, No. 1, pp. 136-143, 1993.

[5] J. M. Guerrero, L. G. de Vicuna, J. Matas, M. Castilla and J. Miret, "A wireless controller to enhance dynamic performance of parallel inverters in distributed generation systems," IEEE Trans. Power Electronics, Vol. 19, No. 5, pp. 1205-1213, 2004.

[6] R. Majumder, A. Ghosh, G. Ledwich and F. Zare, "Load sharing and power quality enhanced operation of a distributed microgrid," IET Renewable Power Generation, Vol. 3, No. 2, pp. 109-119, 2009.

[7] J. G. Slootweg and W. L. Kling, "Impacts of distributed generation on power system transient stability," Power Engineering Society Summer Meeting, 2002 IEEE Vol. 2, No. , pp. 862-867, 2002.

[8] M. N. Marwali, M. Dai and A. Keyhani, "Stability Analysis of Load Sharing Control for Distributed Generation Systems," IEEE Trans. Energy Conversion, Vol. 22, No. 3, pp. 737-745, 2007.

[9] T. Suntio, M. Hankaniemi and M. Karppanen, "Analysing the dynamics of regulated converters," Proc. IEE Electric Power Applications, Vol. 153, No. 6, pp 905-910, 2006

[10] W. Li and L. Tsung-Jen, "Stability and Performance of an Autonomous Hybrid Wind-PV-Battery System," International Conference on Intelligent Systems Applications to Power Systems, pp 1-6, 2007.

[11] E.A.A. Coelho, P.C. Cortizo and P.F.D. Garcia, "Small-signal stability for parallel-connected inverters in stand-alone AC supply systems," IEEE Trans. on Industry Applications, Vol. 38, No. 2, pp. 533-542, 2002.

[12] N. Pogaku, M. Prodanovic, T. C. Green, W. L. Kling, and L. Van Der Sluis, "Modeling, Analysis and Testing of Autonomous Operation of an Inverter-Based Microgrid," IEEE Trans. on Power Electronics, Vol. 22, No. 2, pp. 613-625, 2007.

[13] A. Ghosh and A. Joshi, "A new approach to load balancing and power factor correction in power distribution system," IEEE Trans. Power Delivery, Vol. 15, No. 1, pp. 417-422, 2000.

[14] B. D. O. Anderson and J. B. Moore, Linear Optimal Control, Prentice-Hall, Englewood Cliffs, N.J., 1971.

[15] J. J. E. Slotine and W. Li, Applied Nonlinear Control, Prentice-hall, Englewood Cliffs, N.J., 1991.

[16] H. K. Khalil, Nonlinear Systems, 3rd Ed., Prentice-Hall, Upper Saddle River, N.J., 2002.